Journal of Alloys and Compounds 509 (2011) 966–972

Contents lists available at ScienceDirect

Journal of Alloys and Compounds

journal homepage: www.elsevier.com/locate/jallcom

Synthesis, characterization and magnetic properties of La^{3+} added Mg–Cd ferrites prepared by oxalate co-precipitation method

A.B. Gadkari[a,*], T.J. Shinde[b], P.N. Vasambekar[c]

[a] Department of Physics, GKG College, Subash Road, Kolhapur, Maharashtra 416 012, India
[b] Department of Physics, KRP Kanya Mahavidylaya, Isalampur 415 409, India
[c] Department of Electronics, Shivaji University, Kolhapur 416 004, India

ARTICLE INFO

Article history:
Received 6 June 2010
Received in revised form 13 August 2010
Accepted 24 August 2010
Available online 25 October 2010

Keywords:
Chemical synthesis
Magnetization
Grain boundaries
Microstructure
FT-IR

ABSTRACT

Nanosized powders of Mg–Cd–La ferrite synthesized by oxalate co-precipitation method using high purity sulphates are presented. The powder has been characterized by X-ray powder diffraction (XRD), infrared spectroscopy (FT-IR) and scanning electron microscopy (SEM). The phase identification of powder reveals biphasic nature of materials. The lattice constant, X-ray and physical density, porosity, crystallite size, site radii and bond length were directly affected by addition of rare earth ion (La^{3+}) in Mg–Cd ferrite. The crystallite size of the samples lies in the range 25.67–30.55 nm. FT-IR spectra show two absorption bands in the frequency range from 3.5×10^4 to 8.0×10^4 m^{-1} which are attributed to stretching vibration of tetrahedral and octahedral complex Fe^{3+}–O^{2-} respectively. The addition of La^{3+} alters the characters of powder and decreases the grain size which suppresses the abnormal grain growth. The addition of La^{3+} resulted increase in saturation magnetization, remnant magnetization, $4\pi M_s$ and coercivity. Coercivity shows size dependent behavior. Such results are promising ones for high frequency applications.

1. Introduction

Ferrites are interesting materials due to various potential applications for modern technology. The basis for wide range of applications is related to the verity of transition metal cations, which can be incorporated in to the lattice of the parent magnetic structure [1,2]. The spinel ferrites crystallize in to closed packed cubic structure of oxygen ions [3]. The origin of magnetic properties of the spinel oxides is spin magnetic moment of the unpaired 3d electrons of the transition element occupied by the super exchange interaction via the oxygen ions separation. The magnetic properties such as saturation magnetization, Curie temperature are strongly dependent on the distribution of cations and type of doping atoms. These materials are smart and show variety of magnetic structures [4]. The rare earth ions are the promising additives for the improvement of the ferrite properties.

Many research groups have studied the effect of rare earth ions in different ferrites to improve their structural, electrical and magnetic properties [5–12]. The effect of (La^{3+}) lanthanum substitution on the structural, electrical, dielectric and magnetic properties of ferrites has been extensively studied by many authors [13–17]. Ahmed et al. [14] have studied the physical properties of rare earth (Tb, La, Ce, Th) substituted Mn–Zn ferrite. They have reported change in Curie temperature, magnetic moment, electrical resistivity, density and lattice constant by these substitution either by their partial diffusion in the spinel lattice or the formation of the secondary phase on grain boundaries. Kupferling et al. [17] have reported increase in anisotropy with decreasing temperature of La substituted ferrites shows semiconductor behavior. Samy [18] has studied magnetic and electrical properties of R = La, Nd, Sm, Gd substituted Cu–Zn ferrite and reported decrease in saturation magnetization and grain size. An increase in resistivity and porosity of La^{3+} substituted Mg–Cu ferrite has been reported by Rezlescu et al. [19] and further they showed that conduction in ferrite is sensitive to microstructure. Roy et al. [20,21] have studied the magnetization measurements of La^{3+} substituted Ni–Cu–Zn ferrite using different techniques and reported an increase in saturation magnetization, resistivity and permeability.

Therefore in this paper we report structural and magnetic properties of 5% La^{3+} added Mg–Cd ferrites prepared using oxalate co-precipitation method. This method is economical for producing large quantity of small particle which is different from ceramic method. Further it offers good chemical homogeneity, high purity and lower sintering temperature and time as compared to ceramic method.

2. Experimental procedure

Ferrites having general formula $Mg_{1-x}Cd_xFe_2O_4$ (x = 0.0, 0.2, 0.4, 0.6, 0.8 and 1.0) with 5% addition of La^{3+} were synthesized by the oxalate co-precipitation method. The high purity analytical reagent (AR), $MgSO_4 7H_2O$ (purity 99.99%, Sd

* Corresponding author. Tel.: +91 9423814704.
E-mail address: ashokgadkari88@yahoo.com (A.B. Gadkari).

0925-8388/$ – see front matter © 2010 Elsevier B.V. All rights reserved.
doi:10.1016/j.jallcom.2010.08.155

fine), $3CdSO_4 8H_2O$ (purity 99.99%, Sd fine) $FeSO_4 7H_2O$ (purity 99.5%, Thomas Baker) and $La_2(SO_4)_3 8H_2O$ (purity 99.9%, Alafa Aesar) were used as starting materials. These chemicals were weighed in desired stoichiometric proportion and dissolved in distilled water. The pH of the solution was maintained at 4.8 by adding drop wise concentrated H_2SO_4 [5]. For complete ionization of metal sulphates, the resulting solution was heated at 80 °C for 1 h. The precipitating reagent prepared in distilled water was added drop wise to metal sulphate solution and simultaneously was stirred until the process of precipitation is completed.

The process of precipitation can be explained by chemical reaction as below

$$CdSO_4 + 2H_2O + C_2O_4^{--} \rightarrow CdC_2O_4 2H_2O + SO_4^{--} \quad (1)$$

$$MgSO_4 + 2H_2O + C_2O_4^{--} \rightarrow MgC_2O_4 2H_2O + SO_4^{--} \quad (2)$$

$$FeSO_4 + 2H_2O + C_2O_4^{--} \rightarrow FeC_2O_4 2H_2O + SO_4^{--} \quad (3)$$

$$LaSO_4 + 2H_2O + C_2O_4^{--} \rightarrow LaC_2O_4 2H_2O + SO_4^{--} \quad (4)$$

The resultant precipitation was the solid solution of cadmium, magnesium, ferrous and lanthanum oxalates. The precipitate along with solution was digested on sand bath for 1 h in order to settle down the precipitate at bottom of the beaker. The resultant precipitate was filtered using Whatman filter paper no. 41 with the help of suction flask. The precipitate was thoroughly washed with distilled water to remove sulphate ions. The absence of sulphate ion in the filtrate was confirmed with barium chloride test. The co-precipitate product was dried and presintered at 700 °C for 6 h in air. The presintered powder was milled in an agate mortar with AR grade acetone as a base and sintered at 1050 °C for 5 h. The sintered powder was pressed into the pellets of 13 mm diameter by applying pressure of 5.37 N/m^2 using hydraulic pressure machine. Polyvinyl alcohol 2% by weight was used as a binder. The pellets were finally sintered at 1050 °C for 5 h and were allowed to cool naturally.

The structural phase was confirmed by powder X-ray diffractometer (XRD) Philips PW-3710, in 2θ range 20–80° using CuKα radiation (λ = 1.5424 Å). The crystallite size was calculated by Debye Scherrer's formula. The physical density of pelletized samples was measured by using Archimedes principle. The FT-IR absorption spectra of sample were recorded on a Perkin–Elmer spectrum one spectrometer by KBr pellet technique between 3.5×10^4 m^{-1} and 8×10^4 m^{-1}. The microstructure of fractured surface of the pellets was observed with a scanning electron microscope (SEM) (JEOL–JSM 6360 model, Japan). The magnetization measurements were carried out at room temperature by using high field hysteresis loop tracer Magneta make Mumbai.

3. Results and discussion

3.1. Characterization

The X-ray diffraction patterns of 5% La^{3+} added Mg–Cd ferrites are shown in Fig. 1. The planes corresponding to (2 2 0), (3 0 0), (3 1 0), (3 1 1), (4 0 0), (4 1 1), (4 2 2), (3 3 3)/(5 1 1), (4 4 0) and (5 3 3) reflections have been observed. All the samples show cubic spinel structure with orthoferrite phase. The orthoferrite phase ($LaFeO_3$) is detected in all the sintered samples. It has been established that secondary phase is formed when La^{3+} is added for Fe^{3+} [22]. Similar orthorhombic distortions in La^{3+} substituted Mg–Cu [19] and Gd^{3+} substituted Cu–Cd [23] ferrites have been reported. We have already reported the orthoferrite behavior of Y^{3+} and Sm^{3+} added Mg–Cd ferrite [5,24]. The lattice constant 'a' is calculated for prominent peak (3 1 1) using Bragg's equation (Table 1). The lattice constant of $MgFe_2O_4$ and $CdFe_2O_4$ have been calculated as 8.36 Å and 8.70 Å respectively, which are very close to literature value [24,25]. The relatively larger value of lattice constant for $CdFe_2O_4$ as compared to $MgFe_2O_4$ is due to the larger ionic radius of Cd^{2+} than Mg^{2+}. The variation of lattice constant of Mg–Cd ferrites with Cd^{2+} content and La^{3+} addition is presented in Fig. 2. It is seen that, the lattice constant increases with increase in Cd^{2+} content and shows non linear behavior. This may be due to cadmium, having larger ionic radius which when substituted resides on tetrahedral (A) site of the spinel and displaces proportional amount of Mg^{2+} and Fe^{3+} ion on octahedral (B) site. The reduction in lattice constant is found for La added ferrite due to formation of secondary phase at grain boundary. Similar results for rare-earth substituted ferrites have been reported by others [5,19,24,26].

Table 1
Different parameters estimated from XRD, FT-IR and SEM for 5% La^{3+} added $Mg_{1-x}Cd_xFe_2O_4$ ferrite system.

Cd^{2+} content (x)	Crystallite size D (nm)	Lattice constant a (nm)	Grain size G_a (μm)	X-ray density ρ_x (kg/m^3)	Physical density ρ_p (kg/m^3)	Porosity (P) %	Bond length (Å)		Ionic radii (Å)		Absorption band (m^{-1})	
							A–O	B–O	r_A	r_B	υ_1	υ_2
0.0	29.67	0.8366	0.369	4.89×10^3	4.48×10^3	5.764	2.014	2.032	0.664	0.682	5.71×10^4	4.11×10^4
0.2	29.99	0.8379	0.425	5.27×10^3	4.57×10^3	13.303	2.017	2.036	0.667	0.682	5.70×10^4	4.30×10^4
0.4	30.55	0.8405	0.579	5.60×10^3	4.70×10^3	16.070	2.026	2.045	0.677	0.695	5.79×10^4	4.31×10^4
0.6	30.26	0.8454	0.621	5.91×10^3	4.76×10^3	19.500	2.035	2.054	0.688	0.704	5.71×10^4	4.37×10^4
0.8	30.25	0.8500	0.683	6.20×10^3	4.80×10^3	22.453	2.046	2065	0.696	0.715	5.72×10^4	4.67×10^4
1.0	29.87	0.8706	0.668	6.12×10^3	4.95×10^3	19.073	2.096	2.115	0.746	0.765	5.54×10^4	4.69×10^4

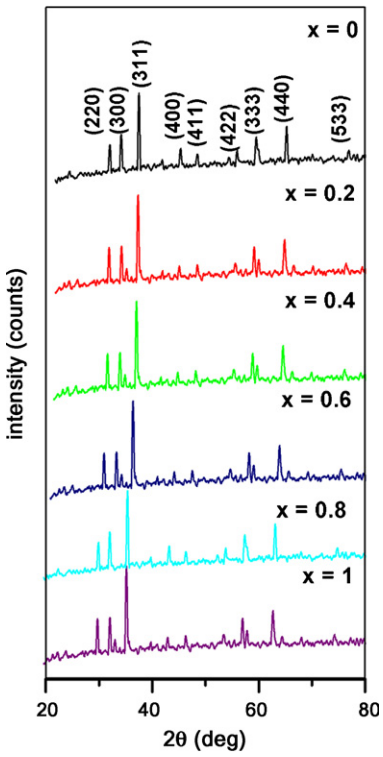

Fig. 1. XRD patterns of 5% La^{3+} added $Mg_{1-x}Cd_xFe_2O_4$ system (x = 0.0, 0.2, 0.4, 0.6, 0.8 and 1.0).

The average crystallite size 'D' is calculated from the (3 1 1) XRD peak using Debye Scherrer's relationship [27,28].

$$D = \frac{0.94\lambda}{\beta \cos\theta} \tag{5}$$

where λ is the wavelength of the incident X-ray; β is the full width at half maxima and θ is the Bragg's diffraction angle. Here $\beta = (\beta_M^2 - \beta_S^2)^{1/2}$, where β_M is the full width at half maximum (FWHM) of the (3 1 1) peak and β_S is the standard instrumental broadening [5]. It is observed that, the crystallite size of the sintered ferrite powder varies from 25.65 to 30.26 nm. The average crystallite size of samples under investigation is smaller than that of samples prepared by ceramic method [25].

The physical density ρ_p of the sample is determined by Archimedes principle using xylene medium. The X-ray density (ρ_x) of the samples is calculated using the relation [28].

$$\rho_x = \frac{8M}{Na^3} \tag{6}$$

where M is the molecular weight of the sample; N is the Avogadro's number and 'a' is the lattice constant. The results are presented in Table 1. The X-ray density is higher than physical density. The physical density of the samples is 83.34% to that of X-ray density. It is also found that, the X-ray and physical density for all compositions of Mg–Cd ferrites increases with increase in cadmium content and are higher than pure ferrite. This is attributed to formation of the $LaFeO_3$ secondary phase which favors the inhabitation of grain growth [29]. The comparison of physical density of pure and 5% La^{3+} added Mg–Cd ferrite is shown in Fig. 3. Thus high density Mg–Cd ferrites can be prepared by oxalate co-precipitation method with addition of rare earth ion.

The results of the porosity 'P' are presented in Table 1. The porosity increases because both physical and X-ray density increases with increase in Cd^{2+} content and it is higher than pure Mg–Cd ferrite due to addition of La^{3+} ions [27]. It is well known that the porosity of the samples results from two sources, intragranular porosity (P_{intra}) and intergranular (P_{inter}) porosity. Thus total porosity 'P' could be written as $P = P_{intra} + P_{inter.}$ The intergranular porosity mostly depends on the grain size and increases with increase in grain size. Therefore, the total porosity leads to the conclusion that the intergranular porosity increases and that the intragranular porosity remains constant with increasing the Cd^{2+} content [30,31]. Such results are in agreement with our previous report of Y^{3+} and Sm^{3+} added Mg–Cd ferrites [5,24].

The bond lengths (A–O, B–O) and ionic radii (r_A, r_B) on tetrahedral and octahedral sites of cubic spinel structure are calculated from relation [32].

$$\text{A–O} = \left(u - \frac{1}{4}\right) a\sqrt{3} \tag{7}$$

$$\text{B–O} = \left(\frac{5}{8} - u\right) a \tag{8}$$

$$r\text{A} = \left(u - \frac{1}{4}\right) a\sqrt{3} - r(O^{2-}) \tag{9}$$

$$r\text{B} = \left(\frac{5}{8} - u\right) a - r(O^{2-}) \tag{10}$$

where a is the lattice constant (Å), $r(O^{2-})$ is the radius of oxygen ion (1.35 Å) and u is the oxygen ion parameter (u = 0.389 for $CdFe_2O_4$ and u = 0.382 for $MgFe_2O_4$). It is observed that the ionic radii and bonds length on A-site are smaller than that of B-site for all samples and increases with increase in cadmium content [5,23].

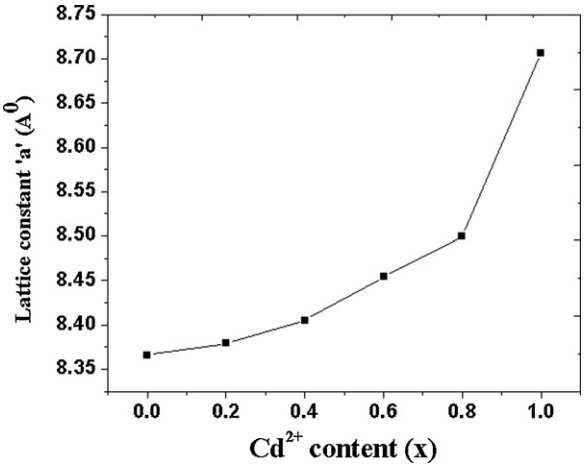

Fig. 2. Dependence of lattice constant 'a' on Cd^{2+} content and La^{3+} addition of ferrite system $Mg_{1-x}Cd_x Fe_2O_4$ (x = 0.0, 0.2, 0.4, 0.6, 0.8 and 1.0).

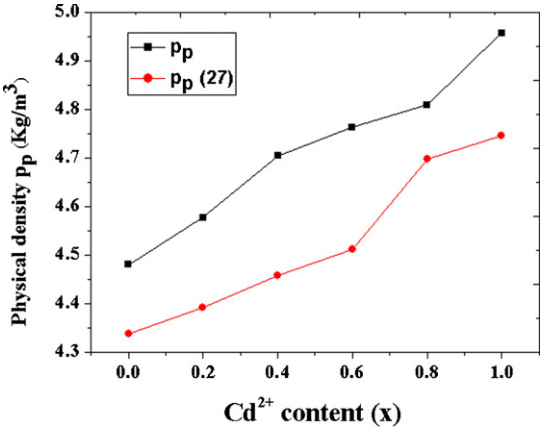

Fig. 3. Comparison of physical densities of pure Mg–Cd and 5% La^{3+} added Mg–Cd ferrite.

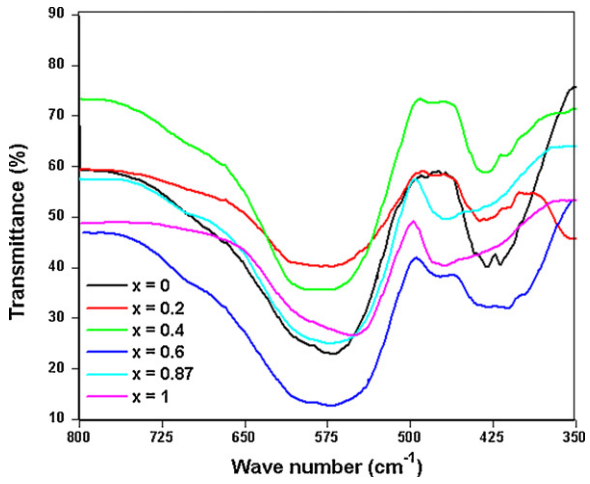

Fig. 4. Infrared absorption spectra of $Mg_{1-x}Cd_x\ Fe_2O_4$ + 5% La^{3+}.

It is seen from Table 1 that as the content of Cd^{2+} in the system $MgFe_2O_4$ increases the presence of Cd^{2+} ions on A-site increases, Since $CdFe_2O_4$ is normal spinel and it occupies A-site only, the bond length increases with more covalent of Cd^{2+} in the system. The increase in bond length is associated with the increase in the lattice constant which is due to increase in Cd^{2+} content. On the addition of La^{3+} it is observed that, bond length and ionic radii are slightly lowered, so that lattice constant is reduced too. This may be due to fact that the ratio of ionic radius of La^{3+} to ionic radius of oxygen (O_2^-) is greater than 0.73. In spinel structure La^{3+} takes position of centre of cube and thus distorts the tetrahedral and octahedral symmetry affecting the lattice constant, ionic radii, bond lengths and central frequency band.

The analysis of FT-IR spectra gives the information about structural transformation and is an important tool to get information about position of ions in the crystal. It also helps to identify the spinel structure as well as chemical substance adsorbed on the surface of particles. The FT-IR spectra of La^{3+} added Mg–Cd ferrite system are shown in Fig. 4. The spectra show two major absorption bands in frequency range $(3.5–8) \times 10^4\ m^{-1}$, which is attributed to stretching vibration of tetrahedral and octahedral group complex Fe^{3+}–O^{2-} [5,33]. The high frequency absorption band (υ_1) is in the range $(5.54–5.80) \times 10^4\ m^{-1}$ and the lower frequency absorption band (υ_2) is in the range $(4.11–4.70) \times 10^4\ m^{-1}$. The high frequency absorption band (υ_1) is caused by scratching vibrations of the tetrahedral metal–oxygen bond and low frequency absorption band (υ_2) is caused by the metal–oxygen vibrations in octahedral sites [34]. The difference in frequencies of υ_1 and υ_2 is due to changes in the bond length Fe^{3+}–O^{2-} at tetrahedral and octahedral site [26,27]. Thus from the X-ray analysis it is found that La^{3+} partially dissolved in material, substitute for Fe^{3+} at octahedral site. The band frequency υ_2 is less as compared to υ_1 band. This is due to the fact that tetrahedral site dimensions are less as compared to the octahedral site dimension and absorption band has inverse relationship with the bond length. The absorption band υ_2 is slightly shifted to higher frequency side due to addition of La^{3+} and is attributed to increase in bond length on B-site. This suggests that, the La^{3+} ions occupy on octahedral B-site. The shift of lattice vibration to the higher frequency could be attributed to the difference in masses between added and displaced ions. In this composition Fe^{3+} ions are replaced by La^{3+} ions which have smaller mass than that of Fe^{3+}. Thus total mass of the lattice decreases leading to an increase in frequency of band [35]. From Fig. 4, it is also observed that the lower frequency absorption band υ_2 broadens with addition of La^{3+} ions and the broadening decreases further with increase in cadmium content. The splitting of the absorption bands is absent in the present case [36].

The SEM microphotographs of fractured surface of the pellets of Mg–Cd–La system are presented in Fig. 5. Each composition deviates from fine structure of pure ferrite $Mg_{1-x}Cd_xFe_2O_4$ [27]. The La^{3+} added Mg–Cd ferrite shows more dark structure which can be attributed to the formation of $LaFeO_3$ secondary phase. The average grain size of the sample is calculated by equation [27] and tabulated in Table 1.

$$Ga = \frac{1.5L}{mn} \tag{11}$$

where L is total test line length, m is the magnification and n is the total number of intercept. It is observed that the average grain size increases with increase in Cd^{2+} composition, due to the higher mobility of Cd^{2+} ions induced in liquid phase sintering [37]. The average grain size lies in the range 0.369–0.668 μm and is smaller than pure Mg–Cd ferrites prepared by oxalate co-precipitation method and ceramic method [25,27]. The addition of 5% La^{3+} in pure Mg–Cd system inhibited the grain growth by about 27%. This decrease in grain size is due to addition of lanthanum, method of preparation and presence of secondary phase. For La^{3+} added sample it is assumed that the La^{3+} ions reside at grain boundaries and causes pressure on the grains. This inhibits the grain growth and decrease in grain size and occurrence of more pores leading to a reduced homogeneity compared with pure ferrite [37,38].

3.2. Magnetization study

The magnetic parameters obtained from magnetic measurement and hysteresis loop are presented in Table 2. Magnetic hysteresis loops for lanthanum added Mg–Cd ferrite are shown in Fig. 6. The parameter saturation magnetization (M_s), remnant magnetization (M_r), M_r/M_s, magnetization in gauss ($4\pi M_s$) and magnetic moment (n_B) increase for $x \leq 0.4$ and thereafter decreasing trend has been observed for $x \geq 0.4$ (Table 2). In Mg–Cd ferrite divalent Mg^{2+} and Fe^{3+} ions occupy both A and B sites [39]. The substitution of magnetic Mg^{2+} for nonmagnetic Cd^{2+} ions increases saturation magnetization with rising x values ($\leq$0.4). The drop in magnetization is observed for $x \geq 0.4$ could be attributed to decrease in A–B type interaction in the Mg–Cd structure. It is observed that the saturation magnetization of La^{3+} (33.41×10^3 emu/kg) added ferrite is higher than pure Mg–Cd ferrites (30.44×10^3 emu/kg). Similar increase in saturation magnetization of La^{3+} substituted Ni–Cu–Zn ferrite has been reported by Roy et al. [20,21].

The variation of saturation magnetization with Cd^{2+} content and La^{3+} addition is shown in Fig. 7. The saturation magnetization increases up to $x = 0.4$ and then goes on decreasing. The decrease in these values may result from the existence of spin canting [22,26,27]. It suggests the existence of canted spins, canting of spins gives rise to Y–K angles which compares the strength of A–B and B–B super exchange interaction. Neel's [39] two sublattice models are applicable for this system for $x \leq 0.4$ and beyond that Niessen's [40] three sub lattice models are predominant. According to Neel's model, A–A, B–B and A–B exchange interactions are possible. The A–B interaction is effective and stronger than the other two. The substitution of Cd^{2+} at A-site successively reduces the Fe^{3+} ions on A-site and equal number of Fe^{3+} ions are transferred to the B-site. This slowly builds up the strength of A–B interaction and hence the magnetization and magnetic moment of the sample increases with Cd^{2+} content. Beyond certain limit of Cd^{2+} content A-site moment is weak to affect B site moments. Therefore B–B interaction become stronger and A–B interaction decreases. The magnetization and magnetic moment on B site decrease. This result is very much similar to our [41] report of magnetic properties of Sm^{3+} added Mg–Cd

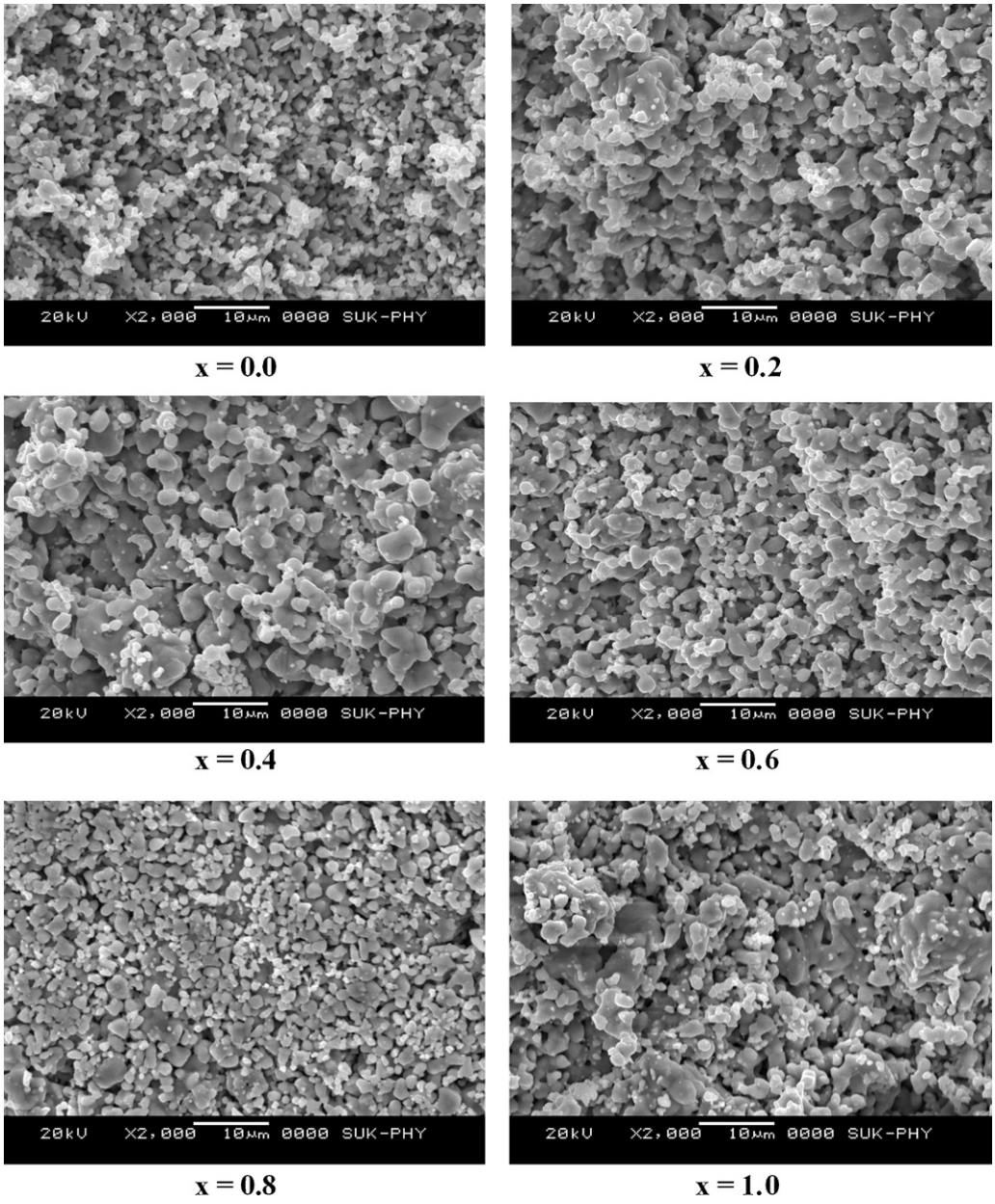

Fig. 5. SEM micrographs of $Mg_{1-x}Cd_xFe_2O_4$ + 5% La^{3+}.

ferrites. The saturation magnetization and magnetic moment is higher than pure Mg–Cd ferrites. This can be attributed to increased density, better structural and chemical homogeneity obtained for ferrite prepared by chemical technique [21]. The higher magnetic moment may be due to smaller free ion magnetic moment (4 μβ) of La^{3+} ion residing on octahedral B-site and results increase in La–Fe interaction on B-site. The cadmium ions occupy A-site, and magnesium and iron ions occupy A and B-sites indifferently [27,37]. Therefore the formula used to propose the cation distribution is

$$(Cd_xMg_\delta Fe_{1-x-\delta})^A[Mg_{1-x-\delta}Fe_{1+x+\delta-0.05}La_{0.05}]^BO_4 \quad (12)$$

The saturation magnetization shows size dependent behavior. The saturation magnetization increases with increase in crystallite size and attains maximum value of 33.41 emu/g at 25.65 nm and

Table 2
Magnetization data of 5% La^{3+} added $Mg_{1-x}Cd_xFe_2O_4$ ferrite system.

Cd $^{2+}$ content (x)	Saturation magnetization M_s (10^3 emu/kg)	Remnant magnetization M_r (10^3 emu/kg)	M_r/M_s	Saturation magnetization M_s (10^6 emu/m^3)	$4\pi M_s$ (Gauss)	Coercive force Hc (Oe)	Magnetic moment n_B (Bohr magneton)	Yafet–Kittel angles $(\alpha_{yk})^0$
0.0	18.01×10^3	5.19×10^3	0.288	80.684×10^6	1013.401	180.19	0.697	0.0
0.2	23.79×10^3	7.53×10^3	0.316	108.898×10^6	1367.769	198.05	0.996	33.62
0.4	33.41×10^3	8.56×10^3	0.256	157.174×10^6	1974.104	327.92	1.504	49.94
0.6	27.02×10^3	6.78×10^3	0.250	128.704×10^6	1616.528	245.13	1.302	65.62
0.8	22.77×10^3	4.78×10^3	0.209	109.505×10^6	1375.389	222.4	1.169	76.05
1.0	2.2×10^3	0.25×10^3	0.113	10.907×10^6	136.994	128.35	0.119	89.31

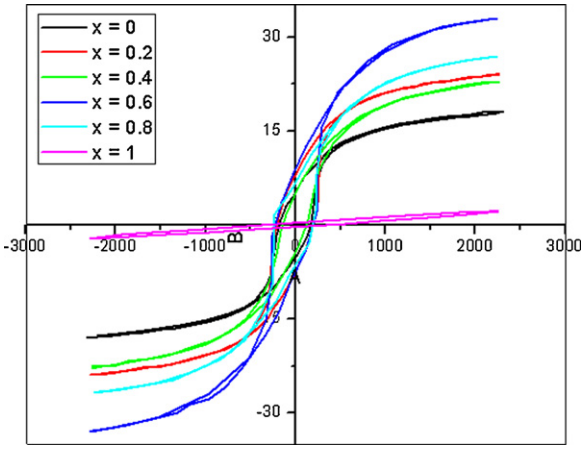

Fig. 6. B–H loops of Mg–Cd ferrite prepared with different Cd^{2+} content and 5% La^{3+} addition.

thereafter decreases with decrease in crystallite size. The decrease of M_s at small size is attributed to the effect of relatively dead or inter surface layer that has low magnetization. This surface effect becomes less effective at small crystallite size. Similar results are reported by others [41,42]. The saturation magnetization of La^{3+} added Mg–Cd ferrite is higher than in pure samples. This is attributed to increase in crystalline size of La^{3+} added samples. Zhao et al. [43] have reported increase in M_s value with increase in crystallite size for rare earth (La, Nd and Gd) substituted Ni–Mn ferrites.

The percentage increase of saturation magnetization in La^{3+} added Mg–Cd ferrites is listed in Table 1. It is found that, for composition $x = 0.4$, the percentage increase of saturation magnetization at room temperature, reaches about 85.5% greater above the unsubstituted $MgFe_2O_4$ ferrites [27]. The percentage increase in saturation magnetization of La^{3+} added Mg–Cd ferrite is higher than that of percentage increase of saturation magnetization (80.11%) of pure Mg–Cd for composition $x = 0.4$. Similar results have been reported by Sattar and Samy [35] for Al^{3+} ions substituted Mn–Ni–Zn ferrites.

The magnetic moment n_B (saturation magnetization per formula unit in Bohr magneton) is calculated from hysteresis loop data recorded at room temperature using the following relation [27]:

$$n_B = \frac{\text{Molecular weight} \times \text{Saturation magnetization}}{5585} \quad (13)$$

The variation in magnetic moment with Cd^{2+} content and La^{3+} addition is presented in Fig. 7. It can be seen from figure that, the magnetic moment increases with the Cd^{2+} content, up to $x = 0.4$ and there after it decreases. The variation of n_B with x can be explained on the basis of the fact that non magnetic Mg^{2+} ions replaces Fe^{3+} ions at tetrahedral A-sites and due to predominant intersublattice A–B super exchange interaction, the net magnetic moment per formula is increased. The decrease of n_B for $x > 0.4$ Cd^{2+} content is found. The n_B values for La^{3+} added Mg–Cd ferrites are higher than pure Mg–Cd ferrites, which is due to increased La–Fe interactions on B-site [7,41,43]. The trend observed is very much similar to that for variation of saturation magnetization in the Mg–Cd ferrites. The values of M_r, Hc, M_r/M_s for all samples are comparable which indicates that anisotropy character for all samples is similar for all the samples, the M_r/M_s ratio is comparable to the mean crystallite size.

The (Y–K) angles for present system are evaluated using the relation [29]

$$n_B = (5 + x)\cos\alpha_{Yk} - 5(1 - x) \quad (14)$$

The dependence of Y–K angles with Cd^{2+} content and La^{3+} addition in Mg–Cd ferrites is presented in Fig. 8. The Y–K angle is zero for magnesium ferrite and finite at and above the composition of $x \geq 0.4$. Therefore we feel that, within the composition $x = 0.2$ to $x = 0.4$ both the Neel's two sublattice model [39] and Y–K model [44] simultaneously exist. With increasing Cd^{2+} content triangular spin arrangement on B-site goes on increasing and beyond $x = 0.4$ Y–K model prevails. It is known that the canting of spins gives rise to Y–K angles which suggests that A–B and B–B super exchange interactions are of comparable strength [44]. It is also observed that, the Y–K angles increases with increase in Cd^{2+} content. This is due to more triangular spin arrangement in the B-site leading to reduction in A–B interaction. The Y–K angles for La^{3+} added samples are lower than pure Mg–Cd ferrites [27]. Similar results are reported by Upadhay et al. [45] for Mg–Cd substituted ferrites.

Fig. 9 shows variation of coercive force with crystallite size of La^{3+} added Mg–Cd ferrites. The coercive force of the nanoparticles increases with increase in crystallite size, attaining maximum value at $x = 0.4$ and decreases further. The coercive force variation of system shows a typical size dependent behavior [41,46]. In our previous paper [41] we have analysed the influence of Sm^{3+} on magnetic properties of Mg–Cd ferrites. Similar size dependent behavior is observed due to addition of La^{3+} in Mg–Cd ferrites. As the particle size increases, the coercivity increases to reach a maximum at a threshold particle size, which could characteristically be described as transformation of multi domain nature to single domain nature, and then decreases. The observed results reveal that the coercivity increases as crystallite size increases, attaining maximum value of 222.4 Oe at 33.41 nm and then decreases with decrease in size of particles. This is attributed to combination of sur-

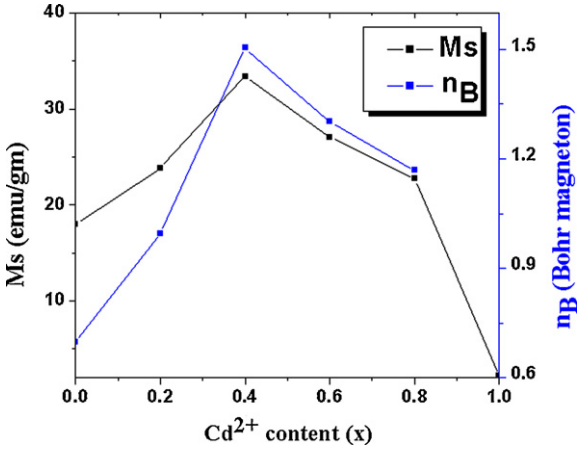

Fig. 7. Dependence of saturation magnetization and magnetic moment with Cd^{2+} content for Mg–Cd + 5% La^{3+} ferrite system.

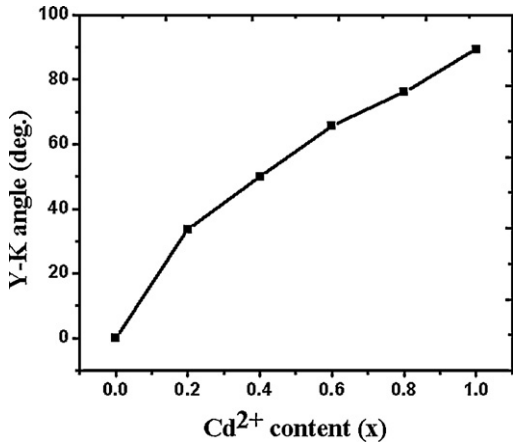

Fig. 8. Variation of Y–K angles with Cd^{2+} content.

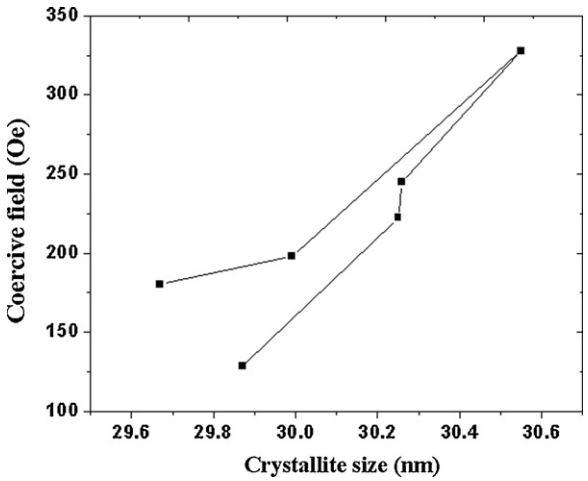

Fig. 9. Dependence of coercivity on crystallite size of 5% La^{3+} added Mg–Cd ferrites.

face effect and its surface anisotropy [47]. The increase in coercive force with increase in crystallite size is due to the enhanced role of the surface anisotropy in comparison with weaker bulk anisotropy. The decrease of Hc at 33.41 nm is due to contribution from development of domain wall in the nanoparticle. Similar results have also been reported earlier [41,48,49]. The improved coercivity in comparision with pure ferrites is attributed to microstructure [49]. The coercivity is a microstructual property which depends on single ion anisotropy, defects, surface effect and non magnetic atoms in the materials [43,50,51].

4. Conclusions

XRD study shows orthoferrite phase in addition to cubic spinel phase by La^{3+}addition in Mg–Cd ferrite. The lattice constant and grain size are found to decrease where as X-ray density, porosity increases and are higher than that of pure Mg–Cd ferrite. This is due to formation of $LaFeO_3$ secondary phase on the grain boundaries. Crystallite size of the samples lies in the nanoparticle range. The grain size (0.36–0.66 μm) increases with increase in Cd^{2+} content and is smaller than pure samples as well as reported by ceramic method. Two absorption bands around frequency $(3.5–8)\times10^4\,m^{-1}$ have been observed from FT-IR. The La^{3+}–O^{2-} band is absent which confirms that La^{3+} ions do not dissolve completely in the spinel phase. The absorption band υ_2 shift to higher frequency side and also broadens, which confirms the occupancy of La^{3+} ions on octahedral B site. The saturation magnetization and magnetic moment increases up to $x = 0.4$ and further decreases. The magnetization study shows the existence of Neel's two sublattice model up to $x = 0.4$ and non collinear spin interaction thereafter. The coercivity and saturation magnetization shows size dependant behavior. The Y–K angles increase with Cd^{2+} content and are reduced by addition of La^{3+} ions. Y–K model exist for all samples except $x = 0$. The reduction in grain size and crystallite size as compared to pure samples improves the structural and magnetic properties.

References

[1] W.C. Kim, S.J. Kim, S.W. Lee, C.S. Kim, J. Magn. Magn. Mater. 22 (2001) 418–442.
[2] J. Smith, H.P.J. Wijn, Ferrite, John Wiely and Sons, New York, 1959.
[3] M.R. Anantharaman, S. Reijne, J.P. Jacobs, H.H. Brongersma, R.H.H. Smiths, K. Seshan, J. Mater. Sci. 34 (1999) 4279–4283.
[4] J. Smiths, Magnetic Properties of Materials, Mc Graw Hill, 1971.
[5] A.B. Gadkari, T.J. Shinde, P.N. Vasambekar, J. Mater. Chem. Phys. 114 (2009) 505–510.
[6] P. Sharma, V. Verma, R.K. Sidhu, O.P. Pandey, J. Alloys Compd. 361 (2003) 257–264.
[7] B.P. Ladgaonkar, C.B. Kolekar, A.S. Vaingankar, Bull. Mater. Sci. 22 (1999) 917–920.
[8] M.Z. Said, D.M. Hemeda, S. Abdel Kader, G.Z. Farag, Turk. J. Phys. 31 (2007) 41–50.
[9] A.A. Sattar, A.M. Samy, J. Mater. Sci. 37 (2002) 4499–4502.
[10] K.K. Bharthi, G. Markandeyulu, J. Appl. Phys. 102 (2008) 07E309.
[11] R.N. Bhomik, R. Ranganathan, J. Alloys Compd. 326 (1–2) (2001) 128–131.
[12] X. Li, F. Zheng, Q.G. Zhou, J. She, Trans. Nonferous Met. Soc. China 17 (2007) 680–684.
[13] A.A. Sattar, A.R. Samy, Phys. Status Solidi (a) 171 (1999) 563–569.
[14] M.A. Ahmed, N. Okasha, M.M. El-Sayed, Ceram. Int. 33 (2007) 49–58.
[15] X. Liu, W. Zhong, S.Y. Zhiya, B. Gu, Y. Du, J. Magn. Magn. Mater. 238 (2002) 207–214.
[16] M.A. Ahmed, E. Ateia, L.M. Salah, A.A. Gamal, Mater. Chem. Phys. 92 (2005) 310–321.
[17] M. Kupferling, R. Grossinger, G. Wiesingers, M. Pieper, M. Reissner, Mag. IEEE Trans. 41 (2005) 3889–3891.
[18] A.M. Samy, J. Mater. Eng. Perform. 12 (2003) 569–572.
[19] N. Rezlescu, E. Rezlescu, C.L. Sava, F. Tudorache, P.D. Popa, Cryst. Res. Technol. 39 (2004) 548–557.
[20] P.K. Roy, B.B. Nayak, J. Bera, J. Magn. Magn. Mater. 298 (2006) 38–42.
[21] P.K. Roy, J. Bera, Mater. Res. Bull. 42 (2007) 77–83.
[22] N. Rezlescu, E. Rezlescu, C. Pasnicu, M.L. Craus, J. Phys. Condens. Matter 6 (1994) 5707–5716.
[23] C.B. Kolekar, A.Y. Lipare, B.P. Ladgaonkar, P.N. Vasambkar, A.S. Vangainkar, J. Magn. Magn. Mater. 247 (2002) 142–146.
[24] A.B. Gadkari, T.J. Shinde, P.N. Vasambekar, Mater. Charact. 60 (2009) 1328–1333.
[25] B.R. Karache, B.V. Khasbardar, A.S. Vaingankar, J. Magn. Magn. Mater. 168 (1997) 292–298.
[26] N. Rezlescu, E. Rezlescu, P.D. Popa, L. Rezlescu, J. Alloys Compd. 275–277 (1998) 657–659.
[27] A.B. Gadkari, T.J. Shinde, P.N. Vasambekar, Mater. Sci. Mater. Elect 21 (2010) 96–103.
[28] B.D. Cullity, Elements of X-ray Diffraction, Addison Wesley pub Co. Inc., 1956, p. 99.
[29] A.F.M. Costa, M.R. Morelli, H.G.A. Kiminam, J. Mater. Sci. 39 (2004) 1773–1778.
[30] A.K.M. Akther Hossian, T.S. Biswas, S.T. Mahmud, T. Yanagida, H. Tanaka, T. Kawai, Mater. Chem. Phys. 113 (2009) 172–178.
[31] A.A. Sattar, H.M. El-Sayed, K.M. El-Shokraly, M.M. El-Tabey, J. Mater. Eng. Perfom. 14 (2005) 99–103.
[32] K.J. Standley, Oxide Magnetic Materials, Oxford at Clarendon Press, London, 1962, p. 24.
[33] O.M. Hemeda, J. Magn. Magn. Mater. 281 (2004) 36–41.
[34] R.D. Waldron, Phys. Rev. 99 (1955) 1727–1735.
[35] A.A. Sattar, H.M. El-Sayed, K.M. Ei-Shokrofy, M.M. El-Tabye, J. Appl. Sci. 5 (2005) 162–168.
[36] O.S. Josyulu, J. Sobhanadri, Phys. Status Solidi 65 (a) (1981) 479–482.
[37] S.A. Mazan, S.F. Mansour, H.M. Zaki, Cryst. Res. Technol. 38 (6) (2003) 471–478.
[38] E. Rezlescu, I. Sachelarie, P.D. Popa, N. Rezlescu, Magn. IEEE Trans. 36 (6) (2000) 3962–3967.
[39] I. Neel, Properties magnetiques des ferrites, Ann. Phys. France, 1948, p. 137.
[40] K.F. Niessen, Physica 19 (1953) 1035–1045.
[41] A.B. Gadkari, T.J. Shinde, P.N. Vasambekar, J. Magn. Magn. Mater. 322 (2010) 3823–3827.
[42] I. Xu, J. Zhang, Y. Lia, B. Jing, S. Cao, J. Magn. Magn. Mater. 288 (2005) 54–59.
[43] L. Zhao, H. Yang, L. Yu, Y. Cui, X. Zhao, S. Feng, J. Mater. Sci. 42 (2007) 686–691.
[44] Y. Yafet, C. Kittel, Phy. Rev. 87 (1952) 290–294.
[45] R.V. Upadhayay, R.V. Mehta, K. Prakash, D. Srinivas, R.R. Pant, J. Magn. Magn. Mater. 201 (1999) 129–132.
[46] W.W. Schude, Y.D. Deet, W.W. Screek, H. Kuhn, C. Lamprey, Sheer (Eds.), Ultra Fine Particles, Wiley, New York, 1963, p. 218.
[47] K. Maaz, A. Mumtaz, S.K. Hasanain, A. Ceylan, J. Magn. Magn. Mater. 308 (2007) 289–295.
[48] M. George, S.S. Nair, A.M. John, P.A. Joy, M.R. Raman, J. Phys. D: Appl. Phys. 39 (2006) 900–910.
[49] J.F. Wang, C.B. Ponton, R. Grossinger, I.R. Harris, J. Alloys Compd. 369 (2004) 170–177.
[50] L. Li, Z. Lan, Z. Yu, K. Sun, Z. Xu, H. Ji, IEEE Trans. Magn. 44 (2008) 2107–2112.
[51] Y. Lishun, Q. Liang, Z. Jingwn, J. Meiyan, J. Liqing, S. Jiaueri, J. Rare Earths 26 (2008) 81–84.